

## Article

# Functionalization of Zeolite NaP1 for Simultaneous Acid Red 18 and Cu(II) Removal

Tomasz Bień<sup>1,2</sup>, Dorota Kołodyńska<sup>3</sup>  and Wojciech Franus<sup>4,\*</sup> 

<sup>1</sup> Faculty of Geology, Geophysics and Environmental Protection, AGH University of Science and Technology, Al. Adama Mickiewicza 30, 30-059 Kraków, Poland; tomasz.bien@op.pl

<sup>2</sup> Biko-Serwis sp. z o.o. sp.k., ul. Zakładowa 13, 26-052 Nowiny, Poland

<sup>3</sup> Department of Inorganic Chemistry, Faculty of Chemistry, Institute of Chemical Sciences, Maria Curie-Skłodowska University, M. Curie Skłodowska Sq. 2, 20-031 Lublin, Poland; d.kolodynska@poczta.umcs.lublin.pl

<sup>4</sup> Department of Construction Materials Engineering and Geoengineering, Faculty of Civil Engineering and Architecture, Lublin University of Technology, Nadbystrzycka 40, 20-618 Lublin, Poland

\* Correspondence: w.franus@pollub.pl

**Abstract:** The efficiency of azo dye Acid Red 18 (AR18) and Cu(II) ions simultaneous removal from an aqueous solution on NaP1CS and NaP1H was investigated, taking into account the effect of the phase contact time, pH, initial concentration, temperature, and interfering ions presence. Zeolite denoted as NaP1CS was modified by chitosan (CS) and zeolite denoted as NaP1H was modified by hexadecyltrimethylammonium bromide (HDTMA). In order to characterize sorption properties of NaP1CS, the obtained sorbent was characterized using Fourier transform infrared spectroscopy (FTIR) and nitrogen adsorption/desorption (ASAP). The kinetic parameters were determined by means of the pseudo first order (PFO), pseudo second order (PSO), and intraparticle diffusion (IPD) kinetic models. To present the adsorption data, three different isotherm models (Langmuir, Freundlich and Dubinin-Radushkevich) were used. The desorption process was also examined. It was found that for sorbent NaP1CS the pseudo second order (PSO) kinetic model and the Langmuir isotherm fitted best the experimental data. Moreover, it was noted that the acidic pH is appropriate to achieve the best sorption properties of NaP1CS for Cu(II) and NaP1H for AR18 and Cu(II). The thermodynamic parameters indicate an endothermic process. The most effective solution for the desorption process was found to be 1 M HCl. The results indicate that simultaneous removal of dye AR18 and Cu(II) on modified zeolite NaP1CS or NaP1H is possible and proceeds with a very good efficiency. The obtained zeolites could effectively adsorb AR18 and Cu(II) simultaneously, but their adsorption abilities were rather different.

**Keywords:** fly ash; zeolite; chitosan; dyes; intermolecular interactions



**Citation:** Bień, T.; Kołodyńska, D.; Franus, W. Functionalization of Zeolite NaP1 for Simultaneous Acid Red 18 and Cu(II) Removal. *Materials* **2021**, *14*, 7817. <https://doi.org/10.3390/ma14247817>

Academic Editor: Alain Moissette

Received: 5 November 2021

Accepted: 15 December 2021

Published: 17 December 2021

**Publisher's Note:** MDPI stays neutral with regard to jurisdictional claims in published maps and institutional affiliations.



**Copyright:** © 2021 by the authors. Licensee MDPI, Basel, Switzerland. This article is an open access article distributed under the terms and conditions of the Creative Commons Attribution (CC BY) license (<https://creativecommons.org/licenses/by/4.0/>).

## 1. Introduction

Nowadays, synthetic dyes are much more often used than natural ones [1]. Large amounts of colored wastewaters are produced by such industries as the textile, paper, and plastic industries [2,3]. Dyes can cause allergies and are often characterized by toxic and carcinogenic properties which impose threat for human health [4,5]. The presence of dyes in surface waters can give negative effects (such as confined access to the light, which results in the inhibition of photosynthesis, thus disrupting proper functioning of aquatic ecosystems) [4,6]. Furthermore, unfortunately synthetic dyes are not degradable and stable, so removal of dyes from wastewaters is an urgent task [7]. Not only the presence of dyes in wastewaters poses a threat to aquatic ecosystems and human health, but also heavy metal ions have negative impact [7,8]. Since industrial wastewaters contain both dyes and heavy metal ions, there is a need to examine the systems containing both pollutants simultaneously.

The largest group of synthetic dyes with one or more azo group ( $-N=N-$ ) contains about half of annual worldwide production of colorants [6,9]. They are used even in the paper, cosmetic, food, and drug industries.

Acid Red 18, denoted as (AR18) and commonly known as Ponceau 4R, Cochineal Red A, or New Coccine is one of the such synthetic azo dyes [10,11]. It is mainly used in the food manufacturing industry as a coloring agent E124 [12]. It is also applicable in the drug, cosmetics and pharmaceutical industries [13]. In many cases it occurs simultaneously with metal ions. There are many known methods of wastewater treatment from both heavy metals and dyes e.g. adsorption, ion exchange, coagulation and flocculation, ozonation, reverse osmosis, membrane filtration, activated sludge, chemical oxidation, electro dialysis, and even monopolar electro-coagulation process [14–16]. Also, advanced oxidation processes (e.g., the Fenton process with formation of ferrous ions nanoscale zero-valent iron (NZVI)) can be used for this aim. According to the study of Nazaria et al. [9], the dye removal efficiency (%S) was about 34% and 98% for  $H_2O_2$  (200 mM) and NZVI/ $H_2O_2$  (NZVI and  $H_2O_2$  concentrations were 2 g/L and 200 mM, respectively), at a contact time of 80 min and pH 3. When the pH value increased to 9, then %S decreased to 12% and 29% for  $H_2O_2$  and NZVI/ $H_2O_2$ , respectively.

However, most of these methods are not sufficiently effective due to the chemical inertness of most dyes. As shown by some studies in the case of exceeding a daily dose AR18 can adversely influence on human health resulting in neurobehavioral effects, intake reproductive toxicity, mutagenic action, and potential carcinogenicity [17]. Dyes also cause eutrophication and interference in ecology and chemical changes in water streams [6]. The World Health Organization (WHO) and Food and Agriculture Organization (FAO) regulate daily consumption of AR18 in an amount less than 4.0 mg/kg.

In the case of Cu(II) ions concentrations in drinking water, they vary widely as a result of variations in water characteristics, such as pH, hardness, and its availability in the distribution system. According to the literature data, it was found that Cu(II) levels in drinking water can range from  $\leq 0.005$  mg/L to  $>30$  mg/L [17]. Therefore, for simultaneous dyes and metal ions removal, adsorption is considered as one of the best techniques due to low cost, effectiveness and easy handling [8,15,18]. For this purpose, carbon based materials (activated carbons, biochars, and polymeric based materials) are used [5,19]. Searching for proper material with good adsorption properties, scientists turned to zeolites.

Zeolites are crystalline aluminosilicates with a skeleton made up of tetrahedral  $SiO_4$  and  $AlO_4$  [7,20,21]. They are characterized by excellent ion exchange, adsorption and catalytic properties owing to a number of channels and pores in their structures [22]. Zeolites have structural negative charge and high affinity for transition metal cations. The chemical composition of the zeolite unit cell is expressed by the formula:  $M_nO \cdot Al_2O_3 \cdot xSiO_2 \cdot yH_2O$ , where M is the cation of an alkali metal,  $n$  is the valence charge, and  $x$  and  $y$  are the integers [23]. The excess negative charge is compensated by ions of sodium, calcium, magnesium and potassium. Synthetic zeolites have significantly better adsorption properties than natural ones [23]. Therefore, they are the object of greater interest. In most cases these materials can be modified by incorporation of various functional groups such as hydroxyl, carboxylic, amine, thiol, phosphate, crown ether, etc. These sorbents are chiefly used for heavy metal ions removal [24–26]. Functional groups grafted to the zeolite matrix improve their selectivity not only towards heavy metal ions but also dyes. To introduce these functionalities, chitosan and HDTMA were used [27].

Chitosan (CS) is a cationic polysaccharide obtained by alkaline N-deacetylation of chitin. However, contrary to chitin, the presence of a large number of amine groups on the chitosan chain increases its adsorption capacity [28]. Protonated amino groups can interact electrostatically with anionic dyes in acidic media. Furthermore, acetamide and hydroxyl groups present in the chitosan can serve as active sites [27]. Thus modification of zeolites by chitosan can improve the ability to remove heavy metals and dyes [29]. Furthermore, chitosan modified glass beads [30], activated clays [31], silica [32], and polymers are well

described [1]. Carbon nanotubes (CNT) were used as a matrix for preparation of CS/CNT composites for dyes removal by Wang et al. [33].

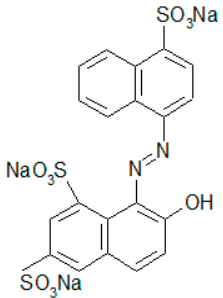
This paper presents zeolite (NaP1) obtained from fly ash by the hydrothermal method and then modified by chitosan (NaP1CS) and hexadecyltrimethylammonium bromide (HDTMA) (NaP1H) as perfect adsorbent for simultaneous removal of AR18 and Cu(II) [34]. It is well-known that the adsorption of cations and especially of anions on the surfaces of zeolites is very limited. However, the anion exchange capacity (AEC) of zeolites can be improved by chemical modification of their surface properties using selected organic compounds such as HDTMA. Therefore, the influence of experimental conditions such as pH, phase contact time, initial concentration, temperature, and interfering ions presence on effectiveness of sorption on chitosan and HDTMA modified zeolite NaP1CS and NaP1H were studied. Moreover, the interactions between AR18 and Cu(II) as well as CS or HDTMA and zeolite were characterized.

## 2. Materials and Methods

### Materials

For synthesis of zeolite there was used fly ash (result of combustion of bituminous coal) from the power generating plant “Kozienice” (Manufacturer, Kozienice, Poland). Zeolite NaP1 was produced based on hydrothermal synthesis of fly ash with sodium hydroxide at atmospheric pressure [35]. Synthesis was performed on a pilot-scale installation for 24 h at 353 K as described in [36]. Chitosan (CS) used in the studies was obtained from Sigma Aldrich (chitosan flakes with the deacetylation degree > 75%). Acid Red 18 (AR18) dye was also purchased from Sigma Aldrich. The general characteristics of the dye used in the research are presented in Table 1. Hexadecyltrimethylammonium bromide (HDTMA) (Merck) was used at amounts equivalent to 1.0 and 2.0 of the NaP1 cation exchange capacity (CEC) according to the procedure described in [34].

**Table 1.** General characteristics of C.I. AR18.

Parameter	Value
Molecular formula	$C_{20}H_{11}N_2Na_3O_{10}S_3$
Molecular weight, g/mol	604.5
COD of 1 g AR18, mg/L	$597 \pm 17$
$\lambda_{max}$ , nm	507
Chemical structure	

The first stage of adsorbent NaP1 modification was to dissolve CS flakes in 1% solution of glycolic acid. It lasted for 24 h using a magnetic stirrer at 1000 rpm at room temperature. In the next stage zeolite NaP1 was added to CS solution, with the ratio of 8:1 and then the mixture was continuously blended using a magnetic stirrer at 1000 rpm for 6 h. To precipitate the resulting product the 1 M NaOH solution was used. Subsequently it was filtered and washed with distilled water to neutral pH, dried and then ground to obtain NaP1CS. In the case of HDTMA modification, zeolite NaP1 was dispersed in about 300 mL of deionized water and the desired amount of HDTMA was slowly added with the ratio of 1:1 and then the mixture was continuously blended using a magnetic stirrer at 1000 rpm for 2 h.

To characterize the sorbents the Fourier transform infrared spectroscopy (FTIR) method is used. FTIR spectra were obtained using a Cary 630 FTIR Spectrometer (Agilent Technologies). The Fourier transform infrared spectra of the samples were measured at  $650\text{--}4000\text{ cm}^{-1}$ . Another analysis was applied to determine such parameters as: specific surface area, micropore surface, micropore volume, total pore volume and average pore diameter. The measurements of  $\text{N}_2$  adsorption/desorption isotherms at 77 K were conducted by ASAP 2420 (Micromeritics Inc., Norcross, GA, USA). To determine the surface morphologies of the sorbents SEM images were taken using the Quanta 3D FEG (FEI) electron microscope.

Stock solution of Cu(II) with the concentration 1000 mg/L was prepared by dissolving proper amounts of  $\text{CuCl}_2 \cdot 2\text{H}_2\text{O}$  (obtained from Avantor Performance Materials Poland S.A.) in distilled water. All of the chemicals used were of analytical grade and used without further purification. The stock solutions of Cu(II) and AR18 were prepared by directly dissolving them in distilled water.

To determine the optimal pH for the sorption of the dye the first tests were performed for the system containing only the dye. The studies were carried out under acidic (pH = 3, 4), almost neutral (pH = 6) and alkaline conditions (pH = 9). For the system containing the AR18 and Cu(II) at concentration (50 mg/L AR18 and 50 mg/L Cu(II)) the effect of pH was studied after adjustment of the initial pH of the solution using 1 M NaOH and 1 M HCl. To determine the effect of pH, 20 mL of the appropriate solution were added to 0.1 g of NaP1, NaP1CS or NaP1H and shaken for 120 min. at room temperature with the amplitude equal 7 and 180 rpm.

In each test, the samples after shaking were filtered and the concentration of Cu(II) was determined by means of the AAS technique using the spectrometer SpectrAA FS-240 (Manufacturer, Varian, Bungarra, Australia). Concentration of the dye solution was measured using UV-Vis spectrophotometer, from Agilent Technologies (Santa Clara, CA, USA), Cary 60 at an optimal wavelength of 506 nm. Figure 1 presents the spectra of dye AR18, at different concentrations.

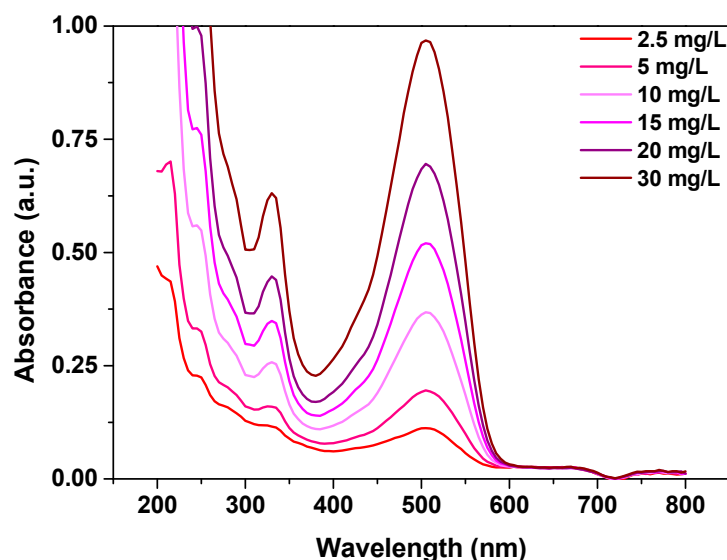


Figure 1. Spectra of AR18 at different concentrations.

Kinetic experiments for AR18 and Cu(II) on NaP1, NaP1CS and NaP1H sorption were carried out by mixing 0.1 g of sorbent with 20 mL two-component solution at concentrations: (50 mg/L AR18 and 50 mg/L Cu(II)) and 100 mg/L AR18 and 100 mg/L Cu(II)). Solutions with sorbents were mixed for the period of time 1–240 min with the shaking amplitude 7 and 180 rpm at 293 K. To calculate the kinetic parameters the pseudo first order, pseudo

second order and intraparticle diffusion kinetic models were used. The pseudo first order equation is generally expressed as follows [36]:

$$\frac{dq_t}{dt} = k_1(q_e - q_t) \quad (1)$$

where  $q_e$  and  $q_t$  are the adsorption capacities at equilibrium and at time  $t$ , respectively (mg/g),  $k_1$  is the rate constant of pseudo first order model (1/min).

After integration and applying the boundary conditions,  $t = 0$  to  $t = t$  and  $q_t = 0$  to  $q_t = q_t$ , this equation is as follows:

$$q_t = q_e(1 - e^{-k_1 t}) \quad (2)$$

The pseudo second order adsorption kinetic rate equation is expressed as follows:

$$\frac{dq_t}{dt} = k_2(q_e - q_t)^2 \quad (3)$$

where  $k_2$  is the rate constant of the pseudo second order model (g/mg min) and  $q_e$  is the adsorption capacity calculated by the pseudo second order model (mg/g).

Integrating Equation (3) and applying the boundary conditions, that is,  $t = 0$  to  $t = t$  and  $q_t = 0$  to  $q_t = q_t$ , gives [27]:

$$q_t = \frac{k_2 q_e^2 t}{1 + k_2 q_e t} \quad (4)$$

Furthermore, the diffusion model was also considered so as to determine the rate-limiting step during the overall adsorption process. One well-known type of diffusion equations used to model the adsorption process is given by Weber-Morris [37]

$$q_t = k_i t^{1/2} + C \quad (5)$$

where  $q_t$  is the adsorption capacity (mg/g) at time  $t$ ,  $t$  is the contact time (min), both  $k_i$  (mg/g min<sup>0.5</sup>) and  $C$  (mg/g) are the Weber–Morris diffusion constants.

In this paper, three different isotherm models were investigated for representing the adsorption data including the Langmuir, Freundlich and Dubinin-Radunshkevich models. The initial AR18 and Cu(II) concentrations were varied from 25–400 mg/L. 20 mL of the appropriate solution was added to 0.1 g of the NaP1CS and NaP1H and mixed at the shaking time 120 min, the shaking amplitude was 7 and 180 rpm at 293 K. The most useful isotherm is the Langmuir isotherm model which indicates monolayer and a homogeneous surface with no interactions between the adsorbate molecules [38]. The Langmuir equation is as follows:

$$q_e = \frac{q_m K_L c_e}{1 + K_L c_e} \quad (6)$$

where  $q_e$  is the adsorption capacity (mg/g) at equilibrium,  $c_e$  is the adsorbate equilibrium concentration in solution (mg/L),  $q_m$  is the monolayer adsorption capacity of the sorbent (mg/g) and  $K_L$  is the Langmuir constant (L/mg) related with the sorption free energy [39]. From the linear plot of  $c_e/q_e$  vs.  $c_e$  both  $q_m$  and  $K_L$  can be determined.

Another model is the Freundlich model, which is an empirical isotherm for sorption on heterogeneous surfaces and multilayer sorption. It is presented in the equation below:

$$q_e = K_F c_e^{1/n} \quad (7)$$

where  $K_F$  (mg/g) is a constant relating the adsorption capacity and  $1/n$  is an empirical parameter relating the adsorption intensity, which varies with the heterogeneity of the material [39]. In turn, the Dubinin–Radushkevich (D–R) isotherm model assumes mul-

tilayer sorption of ions in the most energetically favourable sites of sorbent [40]. The Dubinin-Radunshkevich isotherm is expressed by Equation (8) [41]:

$$q_e = q_s e^{(-Bs^2)} \quad (8)$$

which  $q_s$  and  $B$  constants are obtained from the intercept and slope of the experimental plot of  $\ln q_e$  vs.  $\varepsilon^2$ .  $\varepsilon$  is the Polanyi potential and can be calculated from:

$$\varepsilon = RT \ln \left( 1 + \frac{1}{c_e} \right) \quad (9)$$

where  $R$  is the gas constant (8.314 J/mol K),  $T$  is the temperature (K),  $c_e$  is the equilibrium concentration of the adsorbate (mg/L),  $q_s$  is the sorption monolayer capacity, the parameter  $B$  can be used to calculate the mean free energy of sorption from Equation (10):

$$E = 2B^{-1/2} \quad (10)$$

Temperature effect on adsorption capacity of AR18 and Cu(II) on NaP1CS and NaP1H was studied at 293, 313, and 333 K using 400 mg/L of the initial two-component solution. To explain the effect of temperature on the adsorption process there were used such thermodynamic parameters as the Gibbs's energy change ( $\Delta G^\circ$ ), enthalpy ( $\Delta H^\circ$ ), and entropy ( $\Delta S^\circ$ ). Free energy ( $\Delta G^\circ$ ) was calculated using the following equation [41]:

$$\Delta G^\circ = -RT \ln(K_c) \quad (11)$$

where  $R$  is the gas constant (8.314 J/mol K),  $T$  is the temperature (K), and  $K_c$  is the equilibrium constant equal to  $q_e/c_e$ .  $\Delta H^\circ$  and  $\Delta S^\circ$  were calculated from the slope and intercept of van't Hoff plots of  $\ln K_c$  vs.  $1/T$ .

To determine the interfering ions effect the multi-component solution at the concentrations 50 mg/L AR18 and 50 mg/L Cu(II) with the addition of  $\text{Cl}^-$ ,  $\text{NO}_3^-$ ,  $\text{SO}_4^{2-}$  anions at the concentrations 1000 mg/L were prepared. 20 mL of the appropriate solution was added to 0.1 g of NaP1CS or NaP1H and mixed together at the shaking time 120 min., the amplitude 7, 180 rpm and the temperature 293 K.

Desorption process was examined using 96%  $\text{C}_2\text{H}_5\text{OH}$ , 99.8%  $\text{CH}_3\text{OH}$ , 1 M HCl, 1 M  $\text{CH}_3\text{COOH}$ , 1 M NaOH, and 1 M NaCl solution. 20 mL of solution for desorption was poured into the Erlenmeyer flask containing 0.1 g of NaP1Cs and NaP1H after the adsorption equilibrium of AR18 and Cu(II). The process was carried out for 120 min. at room temperature with the shaking amplitude 7 and 180 rpm. The desorption percentage  $D(\%)$  of AR18 and Cu(II) was defined as [42]:

$$D(\%) = \frac{c_{e(des)}}{c_{e(ads)}} \quad (12)$$

where  $c_{e(des)}$  is the concentration of AR18 and Cu(II) desorbed from NaP1CS or NaP1H (mg/L) and  $c_{e(ads)}$  is the concentration of AR18 and Cu(II) adsorbed on NaP1CS or NaP1H (mg/L).

### 3. Results

#### 3.1. Chemical Characterization of the Materials

The Fourier transform infrared spectra of the samples were measured at 650–4000  $\text{cm}^{-1}$ . Figure 2a presents the spectra of chitosan (CS) and NaP1CS. Figure 2b presents the spectra of hexadecyltrimethylammonium bromide (HDTMA) and NaP1H.

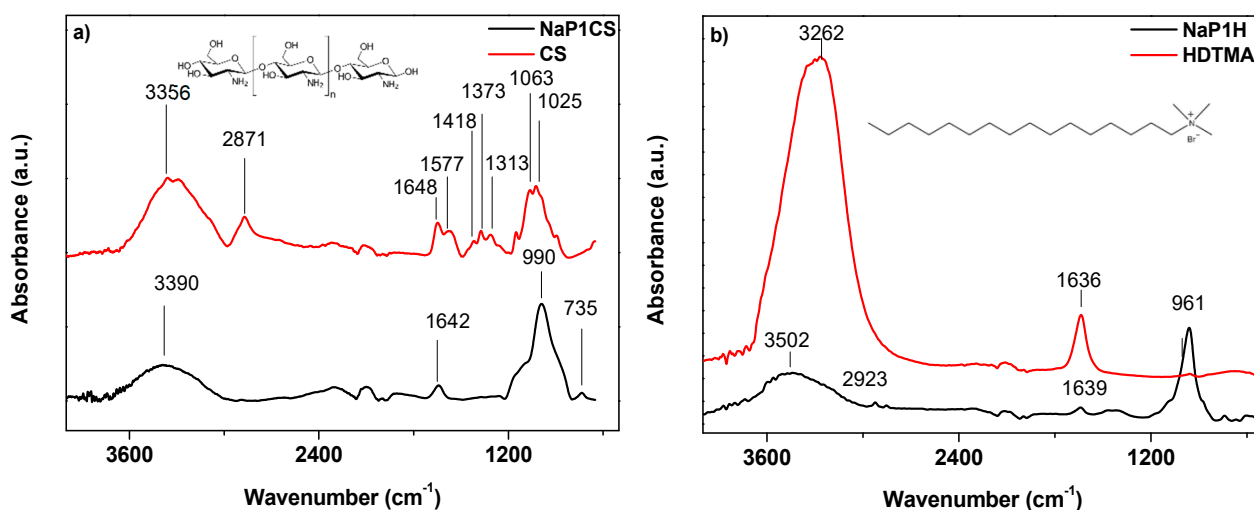


Figure 2. FTIR spectra of (a) CS and NaP1CS as well as (b) HDTMA and NaP1H.

Major adsorption bands for chitosan are situated at  $3356\text{ cm}^{-1}$  ( $-\text{OH}$  and  $-\text{NH}_2$  stretching vibrations),  $2871\text{ cm}^{-1}$  ( $-\text{CH}$  stretching vibrations),  $1648$  and  $1577\text{ cm}^{-1}$  ( $-\text{NH}_2$  bending vibrations),  $1418$  and  $1313\text{ cm}^{-1}$  ( $\text{C}-\text{O}$  stretching vibrations),  $1373\text{ cm}^{-1}$  ( $\text{C}-\text{N}$  stretching vibrations),  $1063$  and  $1025\text{ cm}^{-1}$  ( $\text{C}-\text{O}$  skeletal vibrations) [42]. Appearance of the bands of NaP1CS spectra at  $735$  and  $990\text{ cm}^{-1}$  indicates the presence of  $\text{Al}-\text{O}-\text{Si}$  and  $\text{Si}-\text{O}$  bonds stretching, respectively, derived from zeolite. Moreover, after modification of zeolite with CS, it can be observed in the spectra that the intensities of the hydroxyl peaks and amide peaks decrease and are found at  $3390\text{ cm}^{-1}$  and  $1642\text{ cm}^{-1}$  respectively. In the case of HDTMA modification the following bands were found:  $3502\text{ cm}^{-1}$  and  $2923\text{ cm}^{-1}$  (asymmetric and symmetric vibrations of surfactant ‘head’ suggesting that it possesses the quaternary ammonium groups  $-\text{N}(\text{CH}_3)_3$  as well as at  $1639\text{ cm}^{-1}$  connected with  $\text{CH}_3-\text{N}$  band. It should be noted that it also contains 16 carbons and thus being relatively longer than other quaternary ammonium salts, is usually used for modifying zeolites. As for a role of HDTMA, it is not bound to the silicate surfaces.

Another analysis was applied to determine such parameters as: specific surface area, micropore surface, micropore volume, total pore volume and average pore diameter. Table 2 presents values of surface area, pore size and pore volume. According to the IUPAC classification the  $\text{N}_2$  adsorption/desorption isotherms of NaP1CS belong to IV type isotherm and  $\text{H}_2/\text{H}_3$  hysteresis loop [43]. The mesopore width reported in the literature is 20 to  $500\text{ \AA}$  so the pore distribution curves are typical of mesopores. Analogous results were obtained for NaP1H. Exemplary results for NaP1CS were presented in Figure 3.

Table 2. Surface characteristics of NaP1CS.

Parameter	NaP1	NaP1CS	NaP1H
$S_{\text{BET}}$ ( $\text{m}^2/\text{g}$ )	94	53	29
$V_{\text{mic}}^{\text{a}}$ ( $\text{cm}^3/\text{g}$ )	0.005	0.004	0.003
$S_{\text{mic}}^{\text{a}}$ ( $\text{m}^2/\text{g}$ )	16.0	10.7	8.34
$V_{\text{tot}}^{\text{b}}$ ( $\text{cm}^3/\text{g}$ )	0.28	0.13	0.11
$D_{\text{av}}^{\text{c}}$ ( $\text{\AA}$ )	109.1	111.7	65.4

$S_{\text{BET}}$  is the specific surface area;  $V_{\text{mic}}$  is the micropore volume;  $S_{\text{mic}}$  is the surface of micropores;  $V_{\text{tot}}$  is the total pore volume;  $D_{\text{av}}$  is the average pore diameter; <sup>a</sup> Calculated from t-plot; <sup>b</sup> Determined at  $p/p_0 = 0.99$ ; <sup>c</sup> Barrett, Joyner and Halenda (BJH) model.

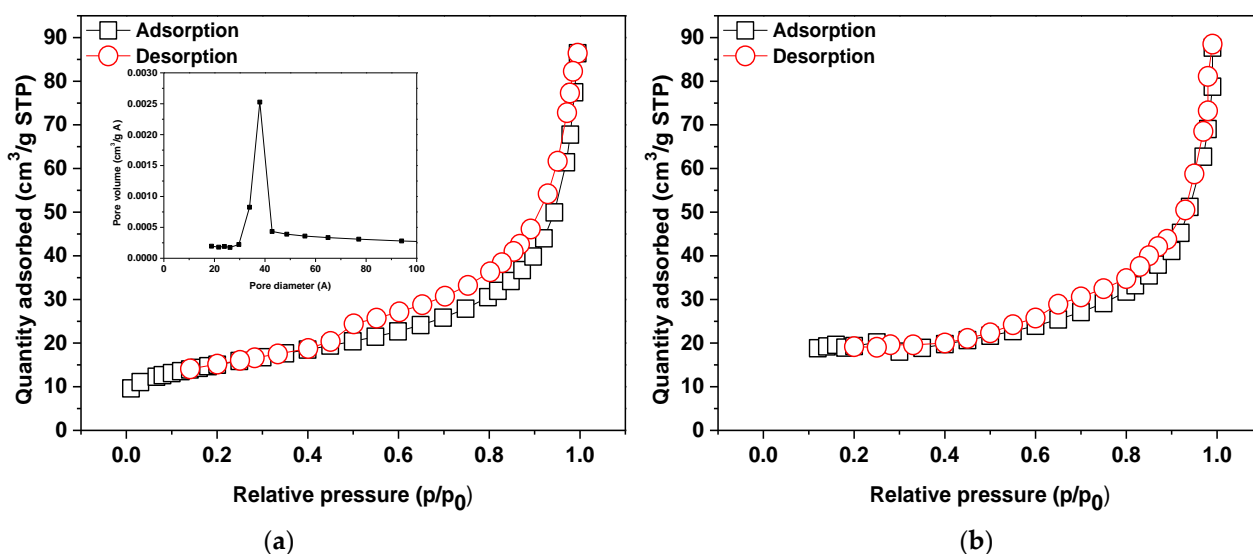


**Figure 3.**  $N_2$  adsorption–desorption isotherms at 77 K and BJH desorption pore size distribution of (a) NaP1CS and (b) NaP1H.

The analysis of textural parameters revealed that both modifications reduce  $S_{BET}$  and porosity of the materials. Consequently, all examined parameters confirm this trend apart from  $D_{av}$ . The surface of the NaP1 zeolite after modification was covered with an organic phase (HDTMA or CS) causing pore blockage. The total pore volume of NaP1 was equal to  $0.28 \text{ cm}^3/\text{g}$ , while after the modification process, the total pore volume achieved the value  $0.13$  and  $0.11 \text{ cm}^3/\text{g}$  for NaP1CS and NaP1H, respectively. However, the average pore diameter increased for NaP1CS to  $111.7 \text{ \AA}$  and decreased for NaP1H to  $65.4 \text{ \AA}$ , in comparison to NaP1 ( $109.1 \text{ \AA}$ ). These data confirm that long chains of HDTMA are more effective in reducing the textural performance of NaP1 than CS.

The SEM images Figure 4 show that the particles of zeolite NaP1 assumed a spherical shape of different sizes and other irregular forms. After modification the surface was covered by CS or HDTMA.

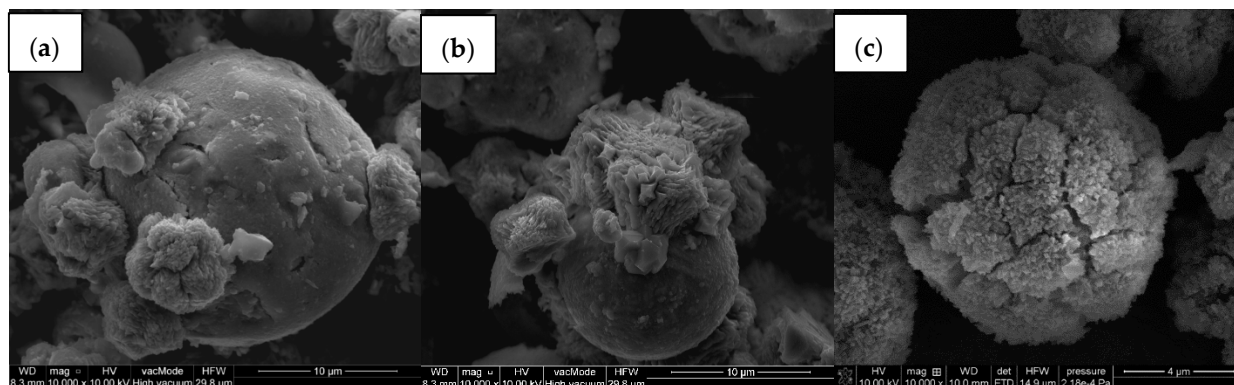


**Figure 4.** SEM photomicrographs of the (a) NaP1, (b) NaP1CS and (c) NaP1H (magnification  $10,000\times$ ).

In the case of XRD pattern for NaP1 and modified NaP1, NaP1H was prepared according to the procedure described in [34]. Muir et al. mentioned that the analysis of the XRD pattern did not show any changes and no additional peaks were observed after the modification of NaP1 by HDTMA. This indicates that the ion exchange process was responsible for the adsorption of surfactant onto the zeolite's surface and thus the structural perturbations did not take place.



### 3.2. pH Effect

The effect of pH on the adsorption was investigated at the AR18 and Cu(II) concentration 50 mg/L for 240 min. The effect of the pH on AR18 and Cu(II) adsorption on NaP1CS and NaP1H was studied over the pH range from 3 to 9. Examining the sorption of the dye, it was observed that the percentage of adsorption (%S) in an acidic medium at pH 3 was equal to 41% for NaP1 and 97% for NaP1CS and 89% for NaP1H while in the alkaline medium at pH 9 the adsorption percentage (%S) decreased (data not presented). The obtained values relate to the  $q_e$  were presented in Figure 5.

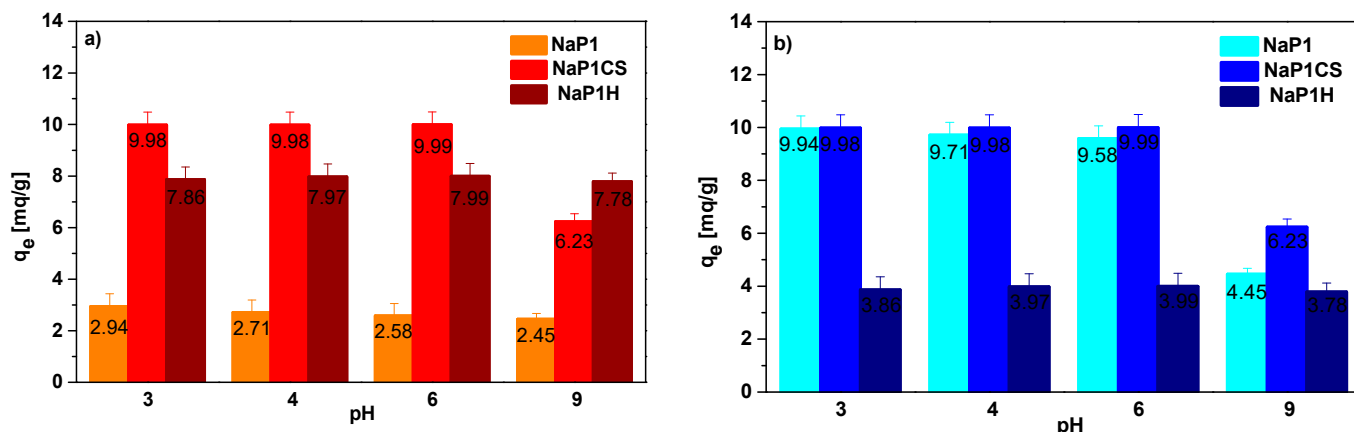
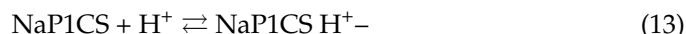


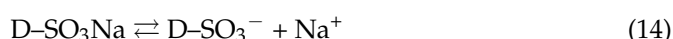
**Figure 5.** Influence of pH on adsorption of (a) AR18 and (b) Cu(II) on NaP1, NaP1CS and NaP1H ( $m = 0.1$  g,  $t = 120$  min,  $A = 7$ , 180 rpm, pH = 3–9).

For zeolite NaP1 after sorption of AR18  $q_e$  values dropped insignificantly from 2.94 mg/g to 2.45 mg/g, whereas for chitosan modified zeolite NaP1CS were higher but also dropped from 9.98 mg/g to 6.23 mg/g. In the case of HDTMA modified zeolite NaP1H they were lower compared to NaP1CS and dropped from 7.86 mg/g to 7.78 mg/g. The adsorption capacity for Cu(II) on NaP1CS and NaP1H do not change with pH value increasing. In the range of pH value from 3 to 6, these values were equal almost 10 mg/g and decreased at pH 9 to 6.23 mg/g for NaP1CS (Figure 5b). At a pH above 9, blue flocs appeared with increasing the pH value of AR18 and Cu(II) solution. This is probably due to the hydrolysis process and Cu(II) hydroxide precipitation. The results indicate that acidic pH is effective in achieving maximum dye removal. This is due to the fact that the pH value influences on CS and HDTMA surface charge. With the reduction of pH, the number of protonated amino functional groups of CS on the NaP1 surface increases that can interact electrostatically with an anionic dye AR18. In alkaline solution, the amine groups of CS are deprotonated, so electrostatic interaction between the NaP1CS and AR18 was reduced and resulted in lower removal efficiency. The mechanism of AR18 adsorption on chitosan modified NaP1 can be illustrated by the following steps:

- Protonation ( $-\text{NH}_3^+$ ) amino groups of chitosan ( $-\text{NH}_2$ ) under acidic conditions (Equation (13))



- Simultaneously dissociation of dye molecule ( $\text{D-SO}_3^-$ ), as shown in Equation (14):



- The electrostatic interactions between  $\text{NaP1CS H}^+$  and  $\text{D-SO}_3^-$  (Equation (15))



It was estimated that the adsorption of Cu(II) can proceed on zeolite modified CS as a result of electrostatic interactions in the acidic media (ion exchange) or metal chelation.

In the case of HDTMA, it not only makes NaP1 surface more hydrophobic but also neutralizes the negative charges. It is well-known that HDTMA bilayer on NaP1 surface affect the AR18 adsorption. The values of HDTMA<sup>+</sup> parameters: diameter 0.4 nm, length 2.3 nm and polar head diameter 0.694 nm compared to NaP1 channels suggest slight changes in external cation exchange capacity. Thus, the possible mechanism of AR18 dye adsorption onto NaP1H occurs only on the outer surface. Examining the two-component solution, it was found that pH change from 3 to 6 has a slight effect on the efficiency of AR18 and Cu(II) sorption as shown in Figure 5. As it can be seen from Figure 5, the maximum sorption of AR18 by NaP1H takes place in acidic condition (pH = 3). This effect of pH can be explained with regards to the interaction between AR18 and HDTMA in terms of surface charge. The AR18 is an acidic dye and its sulfonate moiety contains negative sulfonic groups ( $-\text{SO}_3^-$ ). In acidic condition, a layer of HDTMA on the surface of zeolite increases the positive charges on the external surface of zeolite. Therefore, the strong electrostatic attraction between the positively charged sorption site and oppositely charged groups of the AR18 molecules leads to high adsorption capacity of AR18. The noticeable decrease in the AR18 sorption capacity can be noticed by increasing pH. The appropriate pH value was equal to 6.0. It was found that CS modification NaP1 is characterized by better properties than HDTMA modified and therefore further investigations using HDTMA were not carried out. Summarising, modification of the NaP1 zeolite with chitosan (NaP1CS) increases Cu(II) and AR18 sorption, while modification of the NaP1 zeolite with HDTMA (NaP1H) increases AR18 sorption and decreases Cu(II) sorption.

### 3.3. Effect of Initial Concentration

Since the preliminary results indicated that for NaP1CS the maximum adsorption capacities at simultaneous AR18 and Cu(II) removal were achieved at pH 6, in the next step the influence of initial concentration was tested at this value. Influence of initial concentration of AR18 and Cu(II) on adsorption was examined in the two-component solution at two different concentrations 50 and 100 mg/L. As shown in Figure 6 the adsorption capacity increased with the increasing concentration of AR18 and Cu(II).

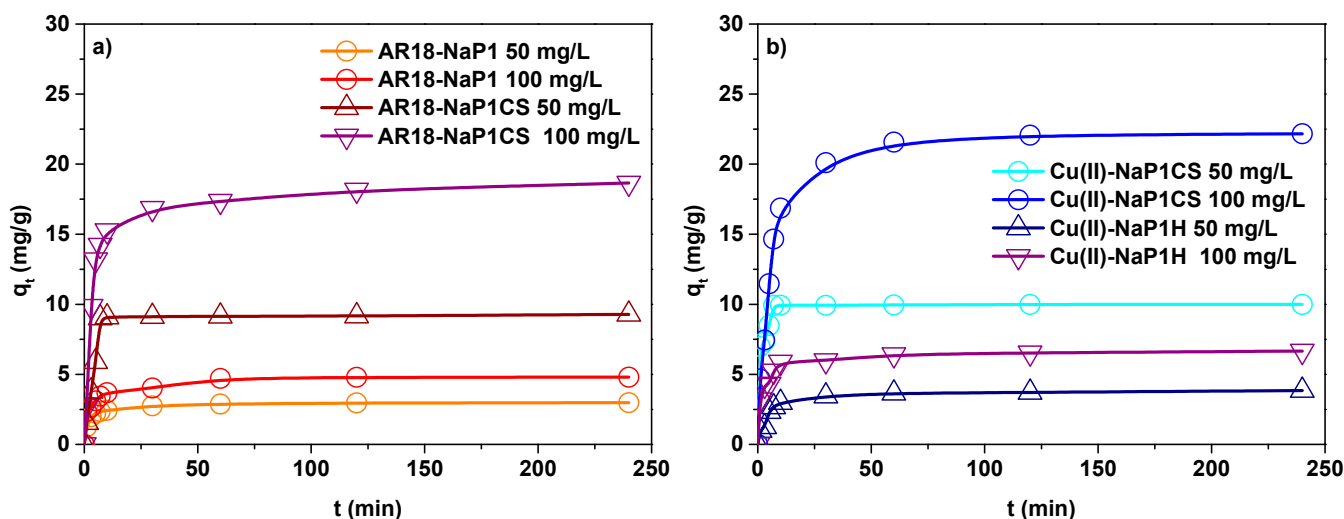


**Figure 6.** Concentration effect of (a) AR18 and (b) Cu(II) adsorption on NaP1CS ( $m = 0.1$  g,  $t = 120$  min,  $A = 7$ , 180 rpm, pH = 6).

### 3.4. Kinetic Effect

The obtained data were modelled using the pseudo first order, pseudo second order and intraparticle diffusion kinetic models. Table 3 presents the parameters for three kinetic models of adsorption of AR18 and Cu(II) on NaP1 and NaP1CS. This data showed that experimentally calculated values of  $q_e$  for the tested concentrations were identical with the theoretical calculated ones in the case of the pseudo second order kinetic model [44].

Furthermore, the values of determination coefficients  $R^2$  were also the highest for the pseudo second order model. This indicates that the pseudo second order kinetic model fits better the adsorption process than the pseudo first order kinetic model. The same trend is observed in many papers. A big difference between the equilibrium constant  $k_2$  and  $k_1$  indicates that the NaP1CS surface was heterogeneous [45].

**Table 3.** Kinetic parameters for the adsorption of AR18 and Cu(II) on NaP1 and NaP1CS.

Adsorbent	Adsorbate	$C_0$ (mg/L)	$q_e$ , exp, (mg/g)	Kinetic Model	Kinetic Parameters		
					$q_{max}$ (mg/g)	$k_1$ ( $h^{-1}$ )	$R^2$
NaP1	AR18	50	2.18	pseudo first order	3.96	0.025	0.75
		100	5.30		2.73	0.023	0.96
	Cu(II)	50	9.91		18.85	0.005	0.80
		100	19.60		2.23	0.035	0.94
NaP1CS	AR18	50	9.94	pseudo second order	1.78	0.012	0.87
		100	19.83		1.84	0.022	0.73
	Cu(II)	50	9.98		99.43	0.023	0.58
		100	19.30		4.05	0.043	0.98
NaP1	AR18	50	2.18	pseudo second order	$q_{max}$ (mg/g)	$k_2$ (g/mg h)	$R^2$
		100	5.30		2.18	0.630	1.00
	Cu(II)	50	9.91		5.39	0.029	0.99
		100	19.60		9.91	1.371	1.00
NaP1CS	AR18	50	9.94	pseudo second order	19.61	0.406	1.00
		100	19.83		9.93	0.173	0.99
	Cu(II)	50	9.98		19.84	0.029	1.00
		100	19.30		9.98	16.632	1.00
NaP1	AR18	50	2.18	intra-particle diffusion	$q_{max}$ (mg/g)	$k_i$ ( $mg/g \cdot min^{0.5}$ )	$R^2$
		100	5.30		2.18	1.35	0.97
	Cu(II)	50	9.91		0.276	2.45	0.90
		100	19.60		0.003	9.85	0.81
NaP1CS	AR18	50	9.94	intra-particle diffusion	0.265	18.71	0.99
		100	19.83		0.111	9.13	0.90
	Cu(II)	50	9.98		0.425	18.27	0.99
		100	19.30		0.028	9.91	0.99
NaP1CS	AR18	50	9.94	intra-particle diffusion	$q_{max}$ (mg/g)	$C$ (mg/g)	$R^2$
		100	19.83		0.111	9.13	0.90
	Cu(II)	50	9.98		0.028	9.91	0.99
		100	19.30		1.011	14.11	0.97

According to the Weber-Morris equation, the adsorption process can be controlled in three different stages. The first stage is the rapid external surface adsorption, while the second step is related to the intraparticle diffusion. The third one is the final equilibrium stage, where intraparticle diffusion starts to slow down [22,46]. This can be due to adsorbate concentration in aqueous solutions and a smaller number of available adsorption sites. The values of  $k_i$  and  $C$  presented in Table 3 were calculated from the second section of the plot. The values of  $k_i$  and  $C$  for the adsorption of AR18 and Cu(II) on NaP1 and NaP1CS increased with the increasing initial AR18 and Cu(II) concentration. However, the intraparticle diffusion model did not fit the adsorption process due to the non-linearity of the plots [32].

### 3.5. Adsorption Isotherms

In the description of experimental data concerning the adsorption of AR18 and Cu(II) on NaP1CS there were investigated three different isotherm models: Langmuir, Freundlich, and Dubinin-Radushkevich. In Table 4 isotherm parameters were collected based on the isotherms presented in Figure 7.

Table 4. Isotherm parameters for AR18 and Cu(II) adsorption on NaP1CS.

Adsorbate	Isotherm	T (K)	Parameters			
AR18	Langmuir	293	$q_m$ (mg/g)	$K_L$ (L/mg)	$R^2$	$R_L$
Cu(II)			74.61	0.390	0.98	0.093
AR18		313	36.04	0.051	0.98	0.440
Cu(II)			81.33	0.355	0.98	0.101
AR18		333	39.47	0.090	0.97	0.307
Cu(II)			123.63	0.189	0.87	0.175
Cu(II)		46.22	0.169	0.98	0.192	
AR18	Freundlich	293	$K_f$ (mg/g)	$n$	$R^2$	
Cu(II)			16.43	2.48	0.53	
AR18		313	7.67	3.57	0.98	
Cu(II)			18.41	1.96	0.88	
AR18		333	9.48	3.67	0.96	
Cu(II)			18.38	1.38	0.97	
Cu(II)		15.16	4.59	0.80		
AR18	Dubinin-Radushkevich	293	$q_s$ (mg/g)	$B$ (mol <sup>2</sup> /kJ <sup>2</sup> )	$R^2$	$E$ (kJ/mol)
Cu(II)			0.003	0.0033	0.52	12.344
AR18		313	1200.354	0.0025	0.98	14.031
Cu(II)			0.007	0.0041	0.91	11.024
AR18		333	1056.565	0.0024	0.97	14.469
Cu(II)			0.017	0.0054	0.97	9.659
Cu(II)		1008.093	0.0018	0.80	16.789	

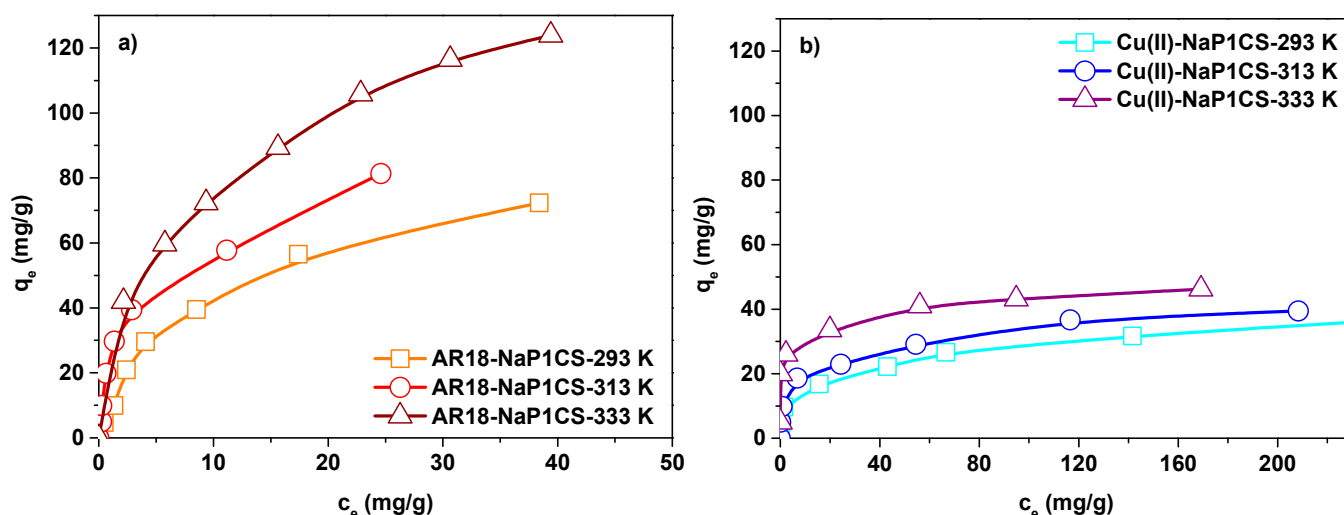


Figure 7. Effect of temperature on the adsorption isotherms of (a) AR18 and (b) Cu(II) adsorption on NaP1CS ( $m = 0.1$  g,  $t = 120$  min,  $c_0 = 10$ – $400$  mg/L,  $A = 7$ ,  $180$  rpm,  $pH = 6$ ).

The equilibrium adsorption capacities for AR18 and Cu(II) increased from  $1.12$  mg/g and  $4.07$  mg/g to  $46.22$  mg/g and  $123.63$  mg/g when AR18 and Cu(II) concentration increased from  $50$  to  $400$  mg/L, respectively. Based on the data,  $R^2$  values for the Langmuir model are higher than for the other model which indicates that the Langmuir model fits best the experimental data. These results show that the surface of the adsorbent is monolayer and homogeneous. Based on the Langmuir isotherms, the values of  $q_m$  for both AR18 and Cu(II) ions increase with the increasing temperature which indicates that higher temperatures facilitate the adsorption process. The maximum values capacity of NaP1CS at  $pH 6.0$ , two-component solution at  $400$  mg/L of AR18(VI) and Cu(II) is  $123.62$  mg/g

as for AR18 and 46.22 mg/g as for Cu(II). It is far more than that of adsorbents reported in [10,37,47]. The  $K_L$  constant of the Langmuir parameters demonstrated the binding affinity between NaP1CS and AR18 and Cu(II). The  $K_L$  values of AR18 range from 0.189 to 0.390 and for Cu(II) from 0.059 to 0.1690. The  $K_L$  values suggested that NaP1CS possess stronger adsorption of AR18 than for Cu(II). Although the determination coefficients  $R^2$  for the Langmuir isotherm concerning the adsorption of AR18 on NaP1CS decrease with the increasing temperature. This points out that at higher temperature the Langmuir isotherm tends toward the Freundlich adsorption model. The nature of adsorption can be determined by  $R_L$  value. The value of  $R_L$  indicates whether the type of isotherm is unfavorable adsorption ( $R_L > 1$ ), favorable adsorption ( $0 < R_L < 1$ ), irreversible adsorption ( $R_L = 0$ ), or linear adsorption ( $R_L = 1$ ) [48]. Also the  $n$  values from the Freundlich model are between 1 and 10 which confirms the favourable character of adsorption [43].

Determined by the Dubinin – Radushkevich isotherm, the value of mean free energy of adsorption  $E$  predicts the mechanism of sorption. Since the values of  $E$  are between 9.659 and 16.789 kJ/mol, the ion exchange mechanism takes place (Table 4) [43].

### 3.6. Effect of Temperature

The easily accessible sorption sites and high surface area of the adsorbent contributed to the rapid adsorption. The AR18 and Cu(II) adsorption capacity for NaP1CS increased with an increase in temperature from 293 to 333 K, indicating better adsorption at higher temperature and an endothermic adsorption process. Similar results were also found concerning adsorption of AR18 on the chitosan/carbon nanotube [33]. In contrast, the AR18 adsorption capacity for NaP1 decreases with an increase in temperature from 293 to 333 K, indicating better adsorption at lower temperature and an exothermic adsorption process. Table 5 presents the thermodynamic parameters for the adsorption of AR18 and Cu(II) on NaP1CS.

**Table 5.** Thermodynamic parameters for Acid Red 18 and Cu(II) adsorption on NaP1 and NaP1CS.

Adsorbent	Adsorbate	$\Delta H^\circ$ (kJ/mol)	$\Delta S^\circ$ (J/mol K)	$\Delta G^\circ$ (kJ/mol)		
				293 K	313 K	333 K
NaP1CS	AR18	29.84	106.3	−18.37	−20.88	−24.99
	Cu(II)	12.49	26.4	−2.15	−13.57	−5.53

The positive  $\Delta H^\circ$  values of AR18 adsorption on NaP1CS and Cu(II) adsorption on NaP1CS indicate that the process is endothermic [48]. The magnitude of the  $\Delta H^\circ$  value for physical adsorption is in the range of 2.1–20.9 kJ/mol while for chemical adsorption 80–200 kJ/mol. The  $\Delta H^\circ$  values of Cu(II) adsorption on NaP1CS indicate physical adsorption processes. The  $\Delta H^\circ$  value of AR18 adsorption on NaP1CS was in the range of neither physical adsorptions nor chemical adsorptions, which can indicate it involves the electrostatic interactions [41]. The negative and went down values of  $\Delta G^\circ$  at all temperatures indicate the spontaneous nature of the adsorption process of AR18 and Cu(II) ions on NaP1CS. The positive values of  $\Delta S^\circ$  mean decrease of the randomness at the solid-solution interface during the adsorption [49].

### 3.7. Interfering Ions Effect

The effects of interfering ions were studied in the presence of chloride, nitrate(V) and sulfate(VI) ions (Figure 8). Their presence hardly affected sorption of AR18 and Cu(II) ions on NaP1CS in opposite to AR18 on NaP1. The greatest influence of the interfering ions was observed in the case of AR18 sorption onto NaP1.

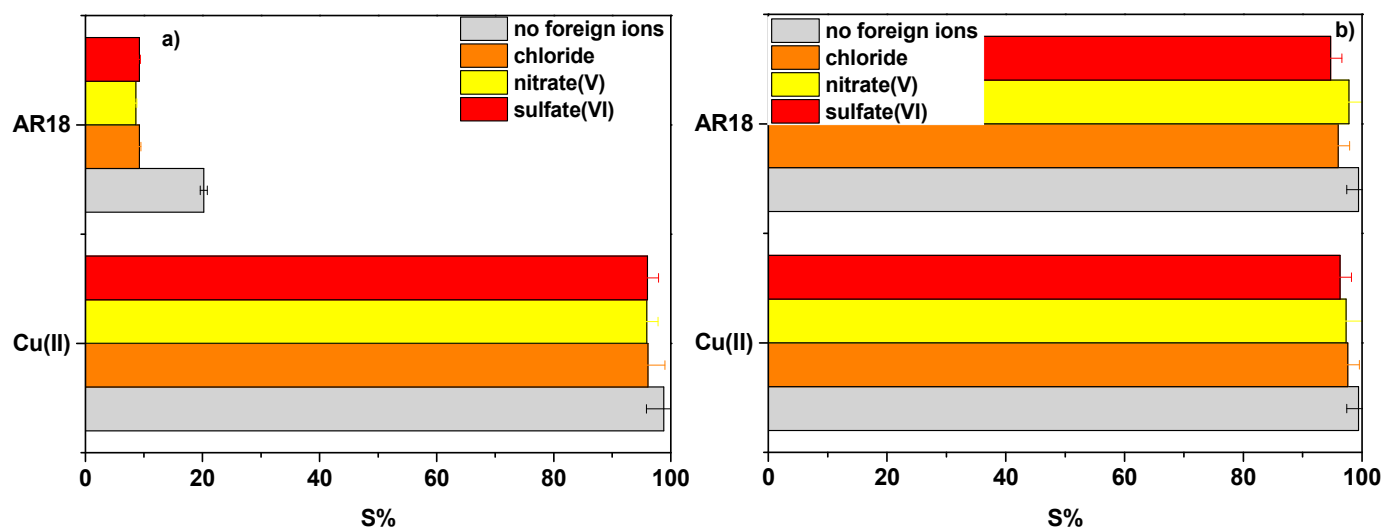


**Figure 8.** Effect of  $\text{Cl}^-$ ,  $\text{NO}_3^-$ ,  $\text{SO}_4^{2-}$  ions on the sorption percentage  $S(\%)$  of AR18 and Cu(II) ions on (a) NaP1 and (b) NaP1CS, ( $m = 0.1$  g,  $t = 120$  min,  $A = 7$ , 180 rpm).

Sorption on NaP1 was mostly affected by the presence of nitrate(V) ions decreasing from 20.2% to 8.6% for the sorption of Acid Red 18 and from 98.8% to 95.9% for the sorption of Cu(II). It can be concluded that even in the presence of chloride, nitrate(V) and sulfate(VI) sorption on NaP1CS can proceed without interference with still very high efficiency as shown in Figure 8. Chitosan modified NaP1 zeolite (NaP1CS) has a high potential in the removal of metal ions and dyes, since it has both amine ( $-\text{NH}_2$ ) and hydroxyl ( $-\text{OH}$ ) group that can serve as active sites. With the reduction of pH, the number of protonated amino functional groups of CS on the NaP1CS surface increases and they can interact electrostatically with an anionic dye AR18. In alkaline solution, the amine groups of CS are deprotonated, so electrostatic interaction between the NaP1CS and AR18 was reduced and resulted in lower removal efficiency. In the case of Cu(II), it was estimated (Fig. 5) that the adsorption of Cu(II) can proceed on zeolite NaP1 and modified NaP1CS as a result of electrostatic interactions (ion exchange) or metal chelation.

### 3.8. Desorption Process

Recovery of heavy metal ions and molecules of dye was made possible as a result of the desorption process. Figure 9 presents the percentage of AR18 and Cu(II) ions desorption DP(%) from NaP1 and NaP1CS. Of all solution used for this purpose the most effective one proved to be 1 M HCl. DP(%) of NaP1 using 1 M HCl were 23.4% and 100% for AR18 and Cu(II) ions, respectively. In contrast, much higher values were obtained with respect to the desorption of NaP1CS and they were 71.3% and 95.2% for AR18 and Cu(II) ions, respectively. The main mechanism of AR18 adsorption on NaP1CS was ion exchange which is generally characterized by high efficiency regeneration [37].

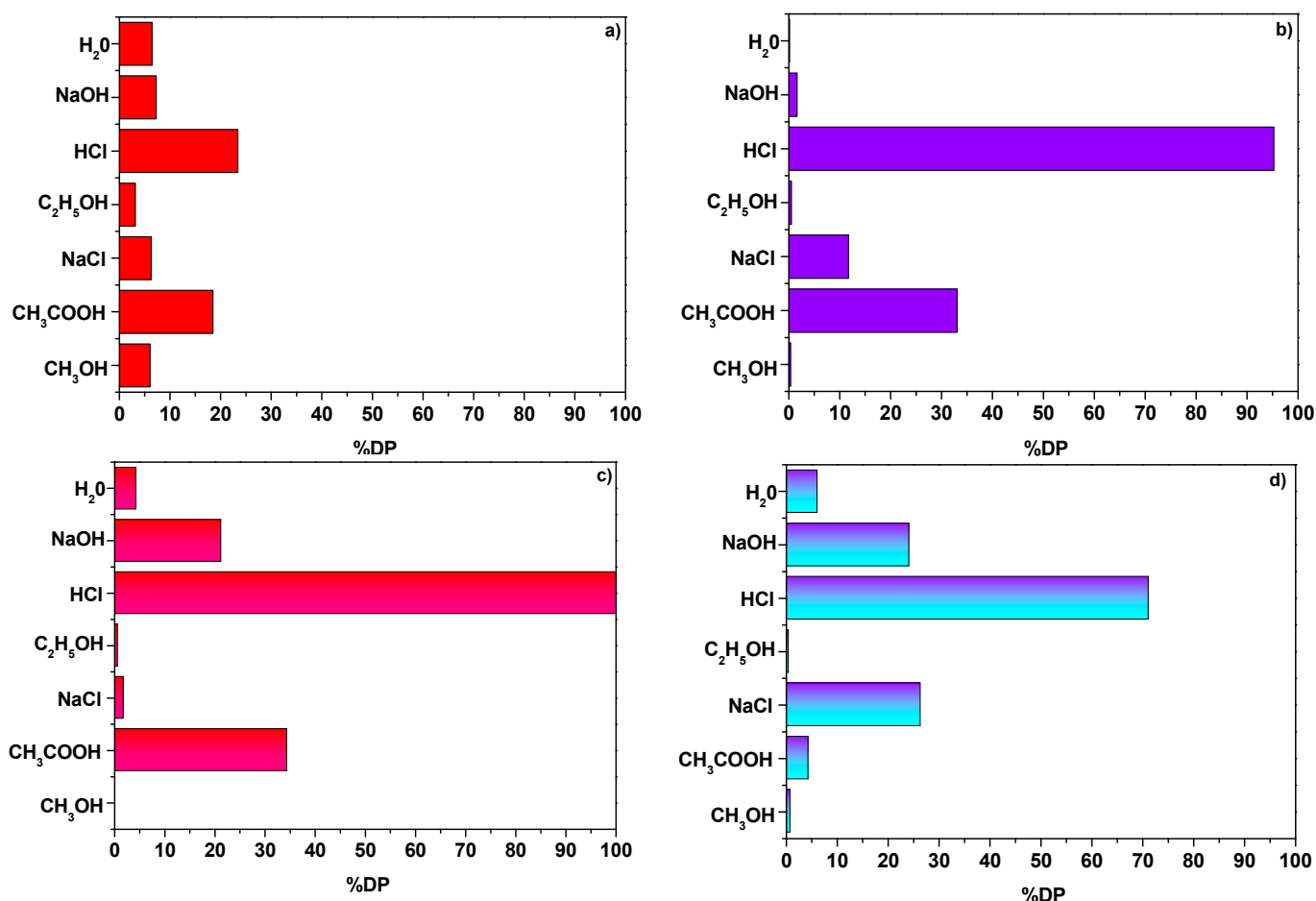


**Figure 9.** (a) Percentage of desorption DP(%) (a) AR18 and (b) Cu(II) from NaP1 as well as (c) AR18 and (d) Cu(II) from NaP1CS ( $m = 0.1$  g,  $t = 120$  min,  $A = 7$ , 180 rpm).

#### 4. Conclusions

In this paper, modified NaP1 zeolite by CS and HDTMA denoted as NaP1CS and NaP1H were investigated to verify the sorption properties compared with those of zeolite NaP1. Acid Red 18 was chosen as a model dye (AR18) and Cu(II) ions as the example of heavy metal ions for removal. Modification of NaP1 by chitosan (CS) and hexadecyltrimethylammonium bromide (HDTMA) improved the sorption properties towards AR18 and the sorption capacity increased almost three times compare to NaP1. However, better results were obtained for CS. Modification of the NaP1 zeolite with chitosan (NaP1CS) increases Cu(II) and AR18 sorption, while modification of the NaP1 zeolite with HDTMA (NaP1H) increases AR18 sorption and decreases Cu(II) sorption. The results showed that the increasing concentration of AR18 and Cu(II) promotes the increase of sorption capacity. The kinetic data were consistent with the pseudo second order kinetic model which is confirmed by the value of correlation coefficient  $R^2$ . The Langmuir isotherms were the best fitted with the equilibrium data so this fact indicates monolayer and homogeneous surface of the adsorbent. The mean free energy of adsorption  $E$  indicates that the ion exchange mechanism takes place. The thermodynamic parameters indicate that temperature increase has a favourable effect on the simultaneous sorption of AR18 and Cu(II) ions. As follows from the results acidic pH is effective in achieving maximum dye removal. The presence of interfering ions did not cause decrease in the effectiveness of the adsorption process which facilitates removal of dyes and heavy metal ions. The 1 M HCl solution proved to be the most effective for the desorption process as the efficiency amounting 71.3% and 95.2% for AR18 and Cu(II) ions, respectively.

**Author Contributions:** Conceptualization, D.K., T.B. and W.F.; methodology, T.B., D.K. and W.F.; validation, D.K. and T.B.; formal analysis, T.B., D.K. and W.F.; investigation, T.B., D.K. and W.F.; writing—original draft preparation, D.K. and W.F.; writing—review and editing, D.K., W.F.; visualization, D.K. and T.B.; supervision, D.K., T.B. and W.F. All authors have read and agreed to the published version of the manuscript.

**Funding:** “The fly ash as the precursors of functionalized materials for applications in environmental engineering, civil engineering and agriculture” no. POIR.04.00-00-14E6/18-00 project is carried out within the TEAM-NET program of the Foundation for Polish Science co-financed by the European Union under the European Regional Development Fund. We acknowledge the participation of students Agata Płaza and Paulina Hałas in our studies.

**Institutional Review Board Statement:** Not applicable.

**Informed Consent Statement:** Not applicable.

**Data Availability Statement:** The data presented in this study are available on request from the corresponding author.

**Conflicts of Interest:** The authors declare no conflict of interest.

## References

1. Ngah, W.S.W.; Teong, L.C.; Hanafiah, M.A.K.M. Adsorption of dyes and heavy metal ions by chitosan composites: A review. *Carbohydr. Polym.* **2011**, *83*, 1446–1456. [[CrossRef](#)]
2. Forgacs, E.; Cserhádi, T.; Oros, G. Removal of synthetic dyes from wastewaters: A review. *Environ. Int.* **2004**, *30*, 953–971. [[CrossRef](#)]
3. Nair, V.; Panigrahy, A.; Vinu, R. Development of novel chitosan-lignin composites for adsorption of dyes and metal ions from wastewater. *Chem. Eng. J.* **2014**, *254*, 491–502. [[CrossRef](#)]
4. Rosales, E.; Pazos, M.; Sanromán, M.A.; Tavares, T. Application of zeolite-*Arthrobacter viscosus* system for the removal of heavy metal and dye: Chromium and Azure B. *Desalination* **2012**, *284*, 150–156. [[CrossRef](#)]
5. Kyzas, G.Z.; Lazaridis, N.K. Reactive and basic dyes removal by sorption onto chitosan derivatives. *J. Colloid Interface Sci.* **2009**, *331*, 32–39. [[CrossRef](#)]
6. Parsa, J.B.; Golmirzaei, M.; Abbasi, M. Degradation of azo dye C.I. Acid Red 18 in aqueous solution by ozone-electrolysis process. *J. Ind. Eng. Chem.* **2014**, *20*, 689–694. [[CrossRef](#)]
7. Hernández-Montoya, V.; Pérez-Cruz, M.A.; Mendoza-Castillo, D.I.; Moreno-Virgen, M.R.A. Bonilla-Petriciolet, Competitive adsorption of dyes and heavy metals on zeolitic structures. *J. Environ. Manag.* **2013**, *116*, 213–221. [[CrossRef](#)] [[PubMed](#)]
8. Kyzas, G.Z.; Lazaridis, N.K.; Kostoglou, M. On the simultaneous adsorption of a reactive dye and hexavalent chromium from aqueous solutions onto grafted chitosan. *J. Colloid Interface Sci.* **2013**, *407*, 432–441. [[CrossRef](#)]
9. Nazari, S.; Yari, A.R.; Mahmodian, M.H.; Reshvanloo, M.T.; Matboo, S.A.; Majidi, G.; Emamian, M. Application of H<sub>2</sub>O<sub>2</sub> and H<sub>2</sub>O<sub>2</sub>/Fe<sup>0</sup> in removal of Acid Red 18 dye from aqueous solutions. *Arch. Hyg. Sci.* **2013**, *2*, 114–120.
10. Thiam, A.; Brillas, E.; Centellas, F.; Cabot, P.L.; Sirés, I. Electrochemical reactivity of Ponceau 4R (food additive E124) in different electrolytes and batch cells. *Electrochim. Acta* **2015**, *173*, 523–533. [[CrossRef](#)]
11. Huang, J.; Zeng, Q.; Wang, L. Ultrasensitive electrochemical determination of Ponceau 4R with a novel ε-MnO<sub>2</sub> microspheres/chitosan modified glassy carbon electrode. *Electrochim. Acta* **2016**, *206*, 176–183. [[CrossRef](#)]
12. Song, Y.Z. Electrochemical reduction of C.I. Acid Red 18 on multi-walled carbon nanotubes and its analytical application. *Dye. Pigment.* **2010**, *87*, 39–43. [[CrossRef](#)]
13. Tanaka, T. Reproductive and neurobehavioural toxicity study of Ponceau 4R administered to mice in the diet. *Food Chem. Toxicol.* **2006**, *44*, 1651–1658. [[CrossRef](#)]
14. Dizge, N.; Aydiner, C.; Demirbas, E.; Kobya, M.; Kara, S. Adsorption of reactive dyes from aqueous solutions by fly ash: Kinetic and equilibrium studies. *J. Hazard. Mater.* **2008**, *150*, 737–746. [[CrossRef](#)]
15. Wang, S.; Ariyanto, E. Competitive adsorption of malachite green and Pb ions on natural zeolite. *J. Colloid Interface Sci.* **2007**, *314*, 25–31. [[CrossRef](#)]
16. Azarian, G.; Nematollahi, D.; Rahmani, A.R.; Godini, K.; Bazdar, M.; Zolghadrnasab, H. Monopolar electro-coagulation process for Azo Dye C. I. Acid Red 18 removal from aqueous solutions. *Avicenna J. Environ. Health Eng.* **2014**, *1*, 33–38. [[CrossRef](#)]
17. Wang, Z.; Zhang, H.; Wang, Z.; Zhang, J.; Duan, X.; Xu, J.; Wen, Y. Trace analysis of Ponceau 4R in soft drinks using differential pulse stripping voltammetry at SWCNTs composite electrodes based on PEDOT:PSS derivatives. *Food Chem.* **2015**, *180*, 186–193. [[CrossRef](#)]
18. Gong, J.L.; Zhang, Y.L.; Jiang, Y.; Zeng, G.M.; Cui, Z.H.; Liu, K.; Deng, C.H.; Niu, Q.Y.; Deng, J.H.; Huan, S.Y. Continuous adsorption of Pb(II) and methylene blue by engineered graphite oxide coated sand in fixed-bed column. *Appl. Surf. Sci.* **2015**, *330*, 148–157. [[CrossRef](#)]



19. Saakshy, A.; Singh, K.; Gupta, A.B.; Sharma, A.K. Fly ash as low cost adsorbent for treatment of effluent of handmade paper industry—Kinetic and modelling studies for direct black dye. *J. Clean. Prod.* **2016**, *112*, 1227–1240. [[CrossRef](#)]
20. Xie, J.; Li, C.; Chi, L.; Wu, D. Chitosan modified zeolite as a versatile adsorbent for the removal of different pollutants from water. *Fuel* **2013**, *103*, 480–485. [[CrossRef](#)]
21. Bandura, L.; Franus, M.; Józefaciuk, G.; Franus, W. Synthetic zeolites from fly ash as effective mineral sorbents for land-based petroleum spills cleanup. *Fuel* **2015**, *147*, 100–107. [[CrossRef](#)]
22. El-Naggar, M.R.; El-Kamash, A.M.; El-Dessouky, M.I.; Ghonaim, A.K. Two-step method for preparation of NaA-X zeolite blend from fly ash for removal of cesium ions. *J. Hazard. Mater.* **2008**, *154*, 963–972. [[CrossRef](#)] [[PubMed](#)]
23. Koshy, N.; Singh, D.N. Fly ash zeolites for water treatment applications. *J. Environ. Chem. Eng.* **2016**, *4*, 1460–1472. [[CrossRef](#)]
24. Panek, R.; Medykowska, M.; Wiśniewska, M.; Szewczuk-Karpisz, K.; Jędruchniewicz, K.; Franus, M. Simultaneous Removal of Pb<sup>2+</sup> and Zn<sup>2+</sup> Heavy Metals Using Fly Ash Na-X Zeolite and Its Carbon Na-X(C) Composite. *Materials* **2021**, *14*, 2832. [[CrossRef](#)] [[PubMed](#)]
25. Panek, R.; Medykowska, M.; Szewczuk-Karpisz, K.; Wiśniewska, M. Comparison of Physicochemical Properties of Fly Ash Precursor, Na-P1(C) Zeolite–Carbon Composite and Na-P1 Zeolite—Adsorption Affinity to Divalent Pb and Zn Cations. *Materials* **2021**, *14*, 3018. [[CrossRef](#)] [[PubMed](#)]
26. Flieger, J.; Kawka, J.; Płaziński, W.; Panek, R.; Madej, J. Sorption of Heavy Metal Ions of Chromium, Manganese, Selenium, Nickel, Cobalt, Iron from Aqueous Acidic Solutions in Batch and Dynamic Conditions on Natural and Synthetic Aluminosilicate Sorbents. *Materials* **2020**, *13*, 5271. [[CrossRef](#)] [[PubMed](#)]
27. Ngah, W.S.W.; Teong, L.C.; Toh, R.H.; Hanafiah, M.A.K.M. Comparative study on adsorption and desorption of Cu(II) ions by three types of chitosan-zeolite composites. *Chem. Eng. J.* **2013**, *223*, 231–238. [[CrossRef](#)]
28. De Alvarenga, E.S.; de Oliveira, C.P.; Bellato, C.R. An approach to understanding the deacetylation degree of chitosan. *Carbohydr. Polym.* **2010**, *80*, 1155–1160. [[CrossRef](#)]
29. Anešić, R.; Veličković, S.J.; Antonović, D.G. Modification of chitosan by zeolite A and adsorption of Bezactive Orange 16 from aqueous solution. *Compos. Part B Eng.* **2013**, *53*, 145–151. [[CrossRef](#)]
30. Vieira, M.L.G.; Esquerdo, V.M.; Nobre, L.R.; Dotto, G.L.; Pinto, L.A.A. Glass beads coated with chitosan for the food azo dyes adsorption in a fixed bed column. *J. Ind. Eng. Chem.* **2014**, *20*, 3387–3393. [[CrossRef](#)]
31. Chang, M.Y.; Juang, R.S. Adsorption of tannic acid, humic acid, and dyes from water using the composite of chitosan and activated clay. *J. Colloid Interface Sci.* **2004**, *278*, 18–25. [[CrossRef](#)]
32. Zhao, H.; Xu, J.; Lan, W.; Wang, T.; Luo, G. Microfluidic production of porous chitosan/silica hybrid microspheres and its Cu(II) adsorption performance. *Chem. Eng. J.* **2013**, *229*, 82–89. [[CrossRef](#)]
33. Wang, S.; Zhai, Y.Y.; Gao, Q.; Luo, W.J.; Xia, H.; Zhou, C.G. Highly efficient removal of Acid Red 18 from aqueous solution by magnetically retrievable chitosan/carbon nanotube: Batch study, isotherms, kinetics, and thermodynamics. *J. Chem. Eng. Data* **2014**, *59*, 39–51. [[CrossRef](#)]
34. Muir, B.; Matusik, J.; Bajda, T. New insights into alkylammonium-functionalized clinoptilolite and Na-P1 zeolite: Structural and textural features. *Appl. Surf. Sci.* **2016**, *361*, 242–250. [[CrossRef](#)]
35. Kunecki, P.; Panek, R.; Koteja, A.; Franus, W. Influence of the reaction time on the crystal structure of Na-P1 zeolite obtained from coal fly ash microspheres. *Microporous Mesoporous Mater.* **2018**, *266*, 102–108. [[CrossRef](#)]
36. Kołodzyńska, D.; Ju, Y.; Franus, M.; Franus, W. Zeolite NaP1 functionalization for the sorption of metal complexes with biodegradable N-(1,2-dicarboxyethyl)-D,L-aspartic acid. *Materials* **2021**, *14*, 2518. [[CrossRef](#)]
37. Song, W.; Gao, B.; Xu, X.; Xing, L.; Han, S.; Duan, P.; Song, W.; Jia, R. Adsorption-desorption behavior of magnetic amine/Fe<sub>3</sub>O<sub>4</sub> functionalized biopolymer resin towards anionic dyes from wastewater. *Bioresour. Technol.* **2016**, *210*, 123–130. [[CrossRef](#)]
38. Hor, K.Y.; Chee, J.M.C.; Chong, M.N.; Jin, B.; Saint, C.; Poh, P.E.; Aryal, R. Evaluation of physicochemical methods in enhancing the adsorption performance of natural zeolite as low-cost adsorbent of methylene blue dye from wastewater. *J. Clean. Prod.* **2016**, *118*, 197–209. [[CrossRef](#)]
39. Subbaiah, M.V.; Kim, D.S. Adsorption of methyl orange from aqueous solution by aminated pumpkin seed powder: Kinetics, isotherms, and thermodynamic studies. *Ecotoxicol. Environ. Saf.* **2016**, *128*, 109–117. [[CrossRef](#)]
40. Alzaydien, A.S.; Manasreh, W. Equilibrium, kinetic and thermodynamic studies on the adsorption of phenol onto activated phosphate rock. *Int. J. Phys. Sci.* **2009**, *4*, 172–181.
41. Boyaci, E.; Eroğlu, A.E.; Shahwan, T. Sorption of As(V) from waters using chitosan and chitosan-immobilized sodium silicate prior to atomic spectrometric determination. *Talanta* **2010**, *80*, 1452–1460. [[CrossRef](#)] [[PubMed](#)]
42. Lin, J.; Zhan, Y. Adsorption of humic acid from aqueous solution onto unmodified and surfactant-modified chitosan/zeolite composites. *Chem. Eng. J.* **2012**, *200–202*, 202–213. [[CrossRef](#)]
43. Ahmad, M.; Manzoor, K.; Venkatchalam, P.; Ikram, S. Kinetic and thermodynamic evaluation of adsorption of Cu(II) by thiosemicarbazide chitosan. *Int. J. Biol. Macromol.* **2016**, *92*, 910–919. [[CrossRef](#)]
44. Azlan, K.; Saime, W.N.W.; Liew, L.A.I. Chitosan and chemically modified chitosan beads for acid dyes sorption. *J. Environ. Sci.* **2009**, *21*, 296–302. [[CrossRef](#)]
45. Wu, Y.; Zhang, S.; Guo, X.; Huang, H. Adsorption of chromium(III) on lignin. *Bioresour. Technol.* **2008**, *99*, 7709–7715. [[CrossRef](#)] [[PubMed](#)]

46. Behnamfard, A.; Salarirad, M.M.; Vegliò, F. Removal of Zn(II) ions from aqueous solutions by ethyl xanthate impregnated activated carbons. *Hydrometallurgy* **2014**, *144–145*, 39–53. [[CrossRef](#)]
47. Shokoohi, R.; Vatanpoor, V.; Zarrabi, M.; Vatani, A. Adsorption of acid red 18 (AR18) by activated carbon from poplar wood—A kinetic and equilibrium study. *E-J. Chem.* **2010**, *7*, 65–72. [[CrossRef](#)]
48. Ngah, W.S.W.; Teong, L.C.; Toh, R.H.; Hanafiah, M.A.K.M. Utilization of chitosan-zeolite composite in the removal of Cu(II) from aqueous solution: Adsorption, desorption and fixed bed column studies. *Chem. Eng. J.* **2012**, *209*, 46–53. [[CrossRef](#)]
49. Liao, B.; Sun, W.Y.; Guo, N.; Ding, S.L.; Su, S.J. Equilibriums and kinetics studies for adsorption of Ni(II) ion on chitosan and its triethylenetetramine derivative. *Colloids Surf. A Physicochem. Eng. Asp.* **2016**, *501*, 32–41. [[CrossRef](#)]